Journal of Materials Chemistry A

ROYAL SOCIETY OF CHEMISTRY

PAPER

View Article Online
View Journal | View Issue

Cite this: J. Mater. Chem. A, 2023, 11, 13708

High-performance piezoelectric nanogenerators based on hierarchical ZnO@CF/PVDF composite film for self-powered meteorological sensor†

Yinhui Li, *[a] Jiaojiao Sun,[a] Pengwei Li, [a] Xuran Li,[a] Jianqiang Tan,[a] Hulin Zhang, [a] Tingyu Li,[a] Jianguo Liang,[b] Yunlei Zhou, [c] Zhenyin Hai *[d] and Jin Zhang*[e]

A high-performance piezoelectric sensor was fabricated for the real-time monitoring of meteorological wind and rainfall. A vertically aligned zinc oxide nanowires (ZnO NWs)@chopped short carbon fiber (CF)/poly(vinylidenefluoride) (PVDF) composite piezoelectric film was prepared by homogeneously distributing nail-raked ZnO@CF in a PVDF matrix by a hydrothermal method and a simple spin-coating method. The crystal structure and morphology were characterized. Vertically aligned and uniform arrays of hexagonal ZnO NWs were grown on the CF surface. The effects of the content of incorporated nail-raked ZnO@CF on the mechanical and electrical performance of ZnO@CF/PVDF were studied systematically. The maximum tensile strength of the ZnO@CF/PVDF composite film reached a value of 77.4 MPa with a content of 4.0 wt% of ZnO@CF. The output voltage and current of a ZnO@CF/PVDF composite film PNG also achieved maximum values of 14.91 V and 1.25 μA with a composite of the same ZnO@CF content. The maximum output power of the ZnO@CF/PVDF composite film PNG is about 7.9 μW with an external load of 10 MΩ. The ZnO@CF/PVDF composite film PNG could charge a capacitor and could instantly drive small electronic devices when the capacitor discharged, and the ZnO@CF/PVDF composite PNG could distinguish wind speed or the falling frequency of water drops. Besides, its excellent washability, durability for over 50 000 cycles and stability after 12 months mean the as-prepared ZnO@CF/PVDF composite film could possibly be used as a meteorological sensor for the real-time monitoring of meteorological conditions for self-driving automobiles.

Received 30th March 2023
Accepted 30th May 2023

DOI: 10.1039/d3ta01886e

rsc.li/materials-a

[a]Micro-Nano System Research Center, College of Information and Computer, Taiyuan University of Technology, Taiyuan 030024, Shanxi, Republic of China. E-mail: liyinhui@tyut.edu.cn

[b]College of Mechanical and Vehicle Engineering, Taiyuan University of Technology, Taiyuan, 030024, Shanxi, Republic of China

[c]Hangzhou Institute of Technology, Xidian University, Hangzhou, 311231, Zhejiang, Republic of China

[d]Department of Mechanical and Electrical Engineering, Xiamen University, Xiamen, 361005, Fujian, Republic of China

[e]Shanxi Bethune Hospital, Shanxi Academy of Medical Sciences, Third Hospital of Shanxi Medical University, Taiyuan, 030032, Shanxi, Republic of China

† Electronic supplementary information (ESI) available. See DOI: https://doi.org/10.1039/d3ta01886e

Li Yinhui received her PhD degree majoring in the Physics and Chemistry of Materials at the University of Chinese Academy of Sciences in 2018. Currently, she is doing postdoctoral research work (2022–2024) at Shanxi Bethune Hospital and she is an assistant Professor in the Micro-Nano System Research Center of the College of Information and Computers of Taiyuan University of Technology. Her research interests focus mainly on flexible piezoelectric sensors or nanogenerators, smart piezoelectric fiber sensors, carbon nanocomposite materials and flexible piezoelectric devices.

1. Introduction

The real-time monitoring of meteorological conditions such as wind and rainfall is of great significance for providing useful information and warning of potential meteorological disasters.[1–3] The real-time monitoring of meteorological information in automobiles is mostly based on meteorological sensors. The traditional monitor sensor used in automobiles is based on optical systems, such as infrared systems or cameras.[4,5] However, the infrared light is reflected for infrared systems and insufficient characteristics of rainfall or wind can be detected for cameras. Therefore, there is a pressing need to develop a new generation of sensors that can with high accuracy and reliability collect meteorological information in various environments.

A piezoelectric nanogenerator (PNG) can convert mechanical energy to electrical signals and detect micro-stress forces generated by wind or rainfall. Recently, PNGs based on zinc oxide (ZnO),[6] barium titanate ($BaTiO_3$),[7] gallium nitride (GaN),[8] lead zirconium titanate (PZT)[9] and lead magnesium niobium titanate (PMNT)[10] *etc.* have been reported and used to perceive variations in micro-stress force. They exhibit high piezoelectric performance for detecting micro pressure, but they are fragile, costly and toxic, greatly limiting their application in the curved surfaces of automobile vehicles and wearable raincoats. Organic piezoelectric materials such as PVDF and its copolymers PVDF-TrFE,[11] polyacrylonitrile (PAN),[12] poly(vinyl chloride) (PVC)[13] and polyamide (PA)[14] are lightweight, flexible, formable and low cost, but the piezoelectric coefficient of a piezoelectric polymer is relatively low (1.0–20 pC N^{-1}).[15] The incorporation of a piezoelectric inorganic material filler into a piezoelectric polymer such as a PVDF matrix is the most extensively studied and cost-effective method to synergistically enhance the output performance and flexibility of a PNG.[16–18]

Different ceramic particles like $BaTiO_3$, ZnO, PZT *etc.* and many other types of filler have been explicitly used for incorporation in a PVDF matrix by researchers.[19–22] Among all the materials used as fillers in a PVDF matrix, ZnO has excellent piezoelectric properties and an easily synthesized design. Recently, Bhunia *et al.* reported an energy harvester based on nano-ZnO/PVDF piezoelectric composite films, and the piezoelectric output voltage was about 4.0 V.[23] Sun *et al.* reported a piezoelectric acoustoelectric nanogenerator based on an electrospun PVDF-ZnO hierarchical composite nanofiber membrane, and an acoustoelectric nanogenerator prepared from it was able to generate a voltage and current of 1.1 V and 1.6 μA.[24] Parangusan *et al.* reported the effect of Co–ZnO fillers on the piezoelectric properties of PVDF-HFP, and a flexible nanogenerator manipulated from the polymer nanocomposite (PVDF-HFP/Co–ZnO) exhibits an output voltage of about 2.8 V.[25] However, the output performance of the ZnO/PVDF flexible composite film is poor, which limits its application in a meteorological sensor.

Various approaches have been employed to improve the output performance of a ceramic/PVDF composite: (i) conductive phase doping, taking carbonaceous material doping as an example, such as carbon black, carbon nanotubes and graphene.[26–28] Doping with carbonaceous materials not only promotes the formation of a conductive path in a piezoelectric material,[29] but also induces the formation of a piezoelectric β-phase of PVDF.[30,31] Short chopped carbon fiber (CF) with excellent intrinsic conductivity and flexibility has been used to supply a good 1D flexible substrate for growing ZnO. (ii) Macro/microstructure design, such as a multilayered construction and carbon-coating method. Nour *et al.* fabricated double-sided ZnO NWs/PVDF using two arrays of ZnO NWs placed in a face-to-face configuration.[32] The maximum output voltage was 2.4 V. Huang *et al.*[33] reported ZnO nanoparticles decorated by sensitizing carbon dots (CDs) through the surface carboxyl functional group of CDs to obtain ZnO@CDs, and then the ZnO@CDs were incorporated in a PVDF-HFP matrix. The output voltage of the ZnO@CDs/PVDF-HFP composite was about 0.65 V which brought a 72% increment compared with a pure PVDF PNG.[33] Poor adhesion of the multilayered structure and agglomeration of ZnO nanoparticles are serious obstacles to an improvement in output performance *via* a traditional incorporation method.[34] Therefore, a new fabrication structure and technology with homogeneous ZnO and carbonaceous materials in a PVDF matrix to prepare a high-performance self-powered meteorological sensor is urgently needed.

Hence, a nail-raked hierarchically structured ZnO@CF composite was synthesized by a facile low-temperature hydrothermal method, and then it was homogeneously distributed in a PVDF matrix to prepare a ZnO@CF/PVDF composite flexible piezoelectric film by a spin-coating process. The effects of the content of incorporated ZnO@CF on the mechanical and electric performance of a ZnO@CF/PVDF composite PNG were systematically investigated. The generated power stored in a capacitor could instantly drive small electronic devices, and the ZnO@CF/PVDF composite PNG could respond to wind speed or the frequency of falling water drops. Besides, the ZnO@CF/PVDF composite film is waterproof, and shows excellent durability and stability. This indicates that a ZnO@CF/PVDF composite PNG could be used as a meteorological sensor for the real-time monitoring of meteorological conditions.

2. Experimental section

2.1 Materials

Zinc nitrate hexahydrate ($Zn(NO_3)_2 \cdot 6H_2O$, AR, 99.0%), hexamethylenetetramine (HMTA, AR, ≥99.0%), zinc acetate dihydrate ($Zn(CH_3COO)_2 \cdot 2H_2O$, AR, 99.0%), isopropanol ($(CH_3)_2CHOH$, AR, 99.7%), sodium hydroxide (NaOH, AR, 99.5%), PVDF (weight-average molecular weight (M_w) = 4.0 × 10^5, 99.5%), *N*,*N*-dimethylformamide (DMF, AR, 99.0%), ethanol (C_2H_6O, AR, 95.0%), acetone (CH_3COCH_3, AR, 99.5%), and all the reagents were purchased from Sinopharm Chemical Reagent Co. Ltd, and used without further purification. Short chopped carbon fiber (CF, length ~1 cm, diameter ~7 μm, tensile modulus ~230 GPa, resistivity ~1.0–1.3 Ω cm^{-1}, density ~1.78 g cm^{-3}) without any adhesive was procured from Carbon Thin Technology Co., Ltd and the SEM images are shown in Fig. S1.†

2.2 Synthesis of ZnO@CF/PVDF composite film

2.2.1 Synthesis of CF coated with layer of ZnO seeds. 0.5 mmol of $Zn(CH_3COO)_2 \cdot 2H_2O$ was dissolved in 460 mL of isopropanol at 50 °C under vigorous stirring to form an aqueous solution. 0.1 mmol of NaOH was dissolved in 40 mL of isopropanol at 50 °C under vigorous stirring for 30 min. These two isopropanol solutions were poured into a beaker at 0 °C at the same time, and then the mixture was vigorously stirred at a heating rate of 2 °C min^{-1} to 65 °C and maintained at 65 °C for 2 h. A stable colloidal suspension of ZnO seeds was obtained. Before CF coating with a ZnO seed layer, CF was cleaned ultrasonically in acetone, ethanol and deionized water, respectively, and then dried at 100 °C for 10 min. After that, the cleaned CF was annealed at 150 °C in an air atmosphere and maintained for 15 min after immersion of CF into the ZnO seed solution for 20 min to grow the ZnO seed layer on the CF. After the immersion and annealing process had been repeated 3 times, CF coated with a ZnO seed layer was obtained.

2.2.2 Synthesis of ZnO NWs array@CF composite fiber. The ZnO NWs were grown on ZnO seed-coated CF *via* a hydrothermal method. In a typical process, 0.42 g of HMTA were dissolved in 60 mL of deionized water at room temperature under vigorous stirring, and then 0.89 g of $Zn(NO_3) \cdot 6H_2O$ was slowly added into the above solution under vigorous stirring for another 30 min at room temperature. The mixture solution was then transferred carefully into a Teflon-lined autoclave, and the ZnO seed-coated CF was immersed into the above as-prepared solution, and then heated at 95 °C for 12 h. After the reaction, the samples were washed with deionized water and ethanol several times to remove residual solvent and dried at 50 °C for 6 h. Finally, the ZnO NW array was assembled on the surface of CF and the ZnO@CF hierarchical composite fiber was obtained. The preparation process of the ZnO@CF hierarchical composite fiber is illustrated in Fig. S2.†

2.2.3 Synthesis of ZnO@CF/PVDF composite film. The composite film of ZnO@CF/PVDF was prepared by a cost-effective solvent casting method. 2.0 g of PVDF was added to 16 mL of DMF solvent under continuous magnetic stirring for 4 h at 70 °C. Various concentrations of the ZnO@CF composite fiber (2.0, 4.0, 6.0, 8.0 wt%) were put into the transparent solution, and a homogenous dispersion was achieved after vigorous magnetic stirring for another 3 h at room temperature. Then, the ZnO@CF/PVDF suspension was dropped on a dried and cleaned ITO glass substrate (2.5 cm × 2.5 cm) by spin coating; after that, the samples were placed on a hot plate at 90 °C for 10 min. The composite films were cured and peeled off quickly. Finally, the composite films were polarized at 60 °C by applying a 1.5 kV m^{-1} electric field for 2 h. For comparison, a PVDF film was synthesized in the same manner but without the addition of ZnO@CF composite.

2.3 Fabrication of ZnO@CF/PVDF composite PNG

The ZnO@CF/PVDF composite film was sandwiched between two copper tapes of 4 × 4 cm^2 and 2 × 4 cm^2 serving as the top and bottom electrodes, respectively. For external connections, two Cu wires were attached on the top and bottom electrodes to measure the output performance. Then, polyethylene terephthalate (PET) films were pasted on both sides of the Cu electrodes using Kapton tape to prevent damage to the ZnO@CF/PVDF composite PNG by repeated mechanical excitation and to make it waterproof and dustproof. A schematic illustration of the process for fabricating the ZnO@CF/PVDF composite PNG is given in Scheme 1.

2.4 Characterization

The morphology and chemical composition of the as-prepared ZnO@CF were characterized using a field emission scanning electron microscope (FESEM, model JEOL JSM-7001, Japan) coupled with an energy dispersive spectroscopy (EDS) system. The crystal structure of the prepared samples was measured by X-ray diffraction (XRD, Rigaku Co., Tokyo, Japan) with Cu $K_{\alpha 1}$ (λ = 1.54060 Å) radiation. The XRD measurements were performed in a 2θ range from 10° to 80° with a scanning speed of 5° min^{-1}. The Raman spectra were recorded using a Holoprobe Kaiser optical spectrometer (VV mode, Renishaw, UK) with a spot size of about 1 μm. A 532 nm laser excitation source with a 5 second integration time per spectrum was focused on the composite films *via* a 50× objective lens. Fourier transform infrared (FTIR) spectra of the composite films were recorded on an FTIR spectrometer (TENSOR 37 spectrophotometer with OPUS 6.0 software, Billerica, MA, USA) from 4000 to 400 cm^{-1} with an average resolution of 32 scans at 4 cm^{-1} using an attenuated total reflection method. The dielectric properties of the composite thin films within the frequency range of 100 Hz–1 MHz were analysed using an LCR tester (E4980AL, Agilent, USA). The polarization–electric hysteresis loop (P–E) was measured with a ferroelectric analyser (RTI-Multi-ferroic of Radiant, USA) with a frequency of 1 Hz at room temperature. The films were polarized by a high-voltage polarization device (ET2673D-4, Entai Co., China). The output open-circuit voltage and short-circuit current of the composite piezoelectric PNG were quantitatively measured by a digital oscilloscope (33522A, Agilent, USA) and a source measurement unit (2400 SMU, Keithley, USA), respectively. The output performance of the ZnO@CF/PVDF composite PNG was measured with a test system platform which was built in our previous work.[35] The frequency of the testing mechanical vibrator was fixed at 10 Hz and the same force was applied.

3. Result and discussion

3.1 Morphology and structure

The morphology of the ZnO@CF hetero-architecture and ZnO@CF/PVDF composite film were characterized by FESEM. SEM images of the dense ZnO NW array grown on CF were taken at different magnifications of 2000 and 30 000 (Fig. 1a and b). A cross-section of the ZnO@CF hetero-architecture is shown in Fig. 1c. The diameter distribution of the corresponding ZnO NWs grown on CF is shown in Fig. 1d. A high-density ZnO NW array was uniformly grown on the surface of CF (Fig. 1a). The high-magnification SEM image of ZnO NWs in the red dashed box in Fig. 1a indicated that the ZnO NWs have a uniform

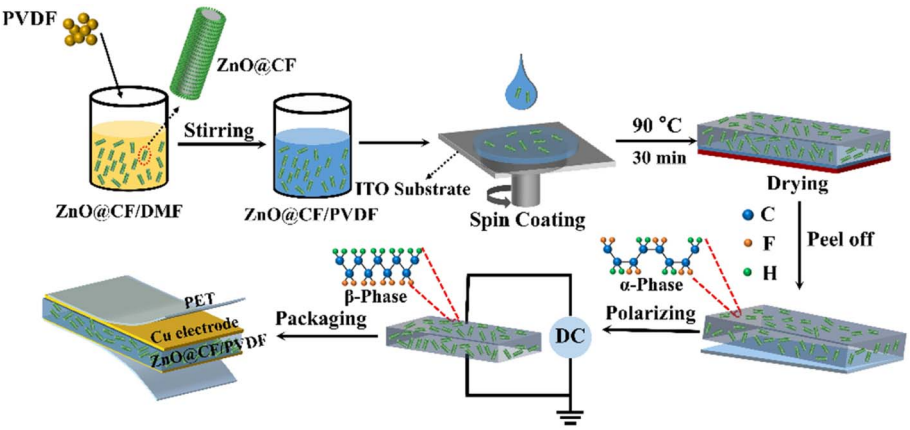

Scheme 1 Fabrication process of the ZnO@CF/PVDF composite PNG.

diameter and a clean surface. A typical regular hexagonal cross-section is observed at the flat ends of a ZnO NW (Fig. 1b). The length of the ZnO NWs is about 6 μm (Fig. 1c) and the hexagon inscribed circle diameter of ZnO NWs ranged from 80 to 220 nm (Fig. 1d). The surface of the ZnO@CF/PVDF composite film was smooth and a small amount of ZnO nanowires were observed in the PVDF matrix and surface (Fig. 1e). From the high-magnification SEM image of ZnO@CF/PVDF in the red dashed box in Fig. 1e, it could be observed that the hetero-architectural ZnO@CF composite was well maintained in the PVDF matrix (Fig. 1f). These results demonstrate that vertically oriented, uniform and dense arrays of hexagonal ZnO NWs have been successfully grown over the entire CF surface and the hetero-architectural morphology of ZnO@CF was well maintained after compositing with PVDF *via* a spin-coating process. The EDS analysis also indicates that ZnO@CF has been successfully compounded with PVDF and the hetero-architectural structure of ZnO@CF has been maintained in the PVDF matrix (Fig. S3 and S4†).

The crystalline structures of ZnO powder, CF, ZnO@CF, pure PVDF and ZnO@CF/PVDF composite films were measured by XRD (Fig. 1e). A large diffraction peak at $2\theta = 20.3°$ corresponding to the (200) facets of the polar β-phase and a small diffraction peak at $2\theta = 18.2°$ corresponding to the (020) facets of the α-phase in the XRD pattern of pure PVDF film can be seen in Fig. 1e. A broad peak at $2\theta = 25.2°$ is attributed to the (002) planes of graphite crystallites in CF. In the case of ZnO powder, the diffraction peaks at 31.8°, 34.4°, 36.3°, 47.5°, 56.6° and 67.8° are assigned to (100), (002), (101), (102), (110) and (103), which are consistent with a hexagonal wurtzite crystal structure and JCPDS card no. 36-1451.[36,37] The characteristic diffraction peaks of CF and ZnO are obviously observed from ZnO@CF and no other diffraction peaks appeared, indicating that the single-crystalline ZnO NWs were successfully grown on CF by

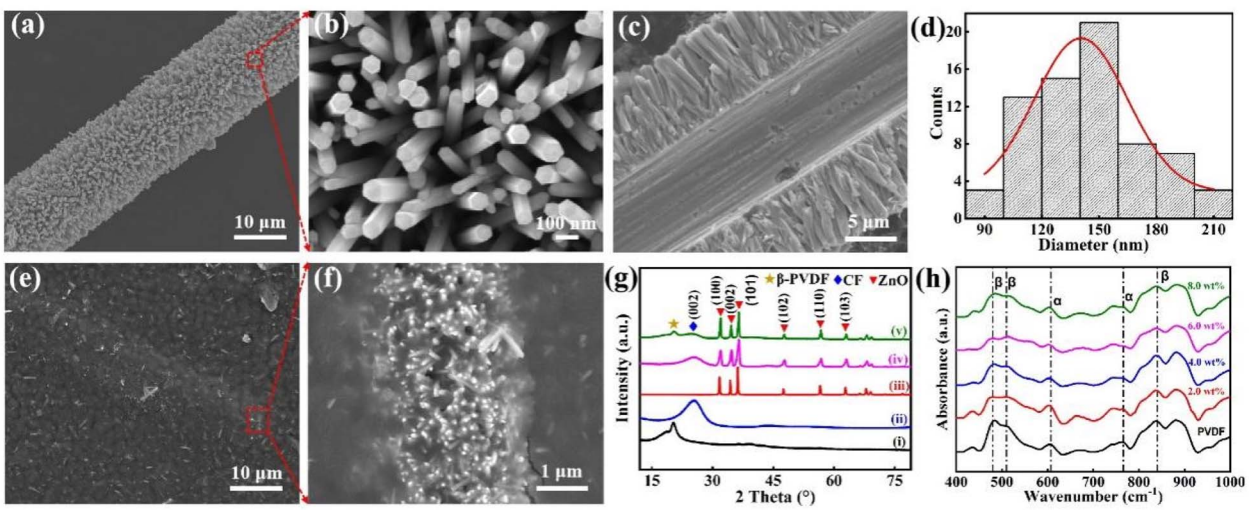

Fig. 1 SEM images of ZnO@CF at different magnifications: (a) ×2000; (b) ×30 000. (c) Cross-section of ZnO@CF hetero-architecture. (d) Diameter distribution of ZnO NWs. (e) SEM images of ZnO@CF/PVDF composite film surface; (f) high-magnification in the red dashed box of (e). (g) XRD patterns of (i) pure PVDF film; (ii) CF; (iii) ZnO powder; (iv) ZnO@CF; (v) ZnO@CF/PVDF composite film. (h) FTIR spectra of pure PVDF film and ZnO@CF/PVDF nanocomposite films with different contents of ZnO@CF.

a hydrothermal method. Furthermore, to confirm the attachment of ZnO NWs on the surface of CF, the Raman spectra of bare CF and ZnO@CF were taken and the results are shown in Fig. S5.† The peaks of the D (~1361 cm^{-1}) and G (~1582 cm^{-1}) bands for ZnO@CF show a slight deviation compared with pure CF (D ~1383 cm^{-1} and G ~1596 cm^{-1}). The intensity value of I_D/I_G for ZnO@CF is 0.95, which is higher than the value for CF of 0.84, indicating that the defects are enhanced owing to ZnO NWs grown on CF and the strong interaction between ZnO and CF at the interface. In a ZnO@CF/PVDF composite film with a content of inorganic filler ZnO@CF of 8.0 wt%, the characteristic diffraction β-phase of PVDF, CF and ZnO were obviously observed, which demonstrated that the ternary composite film had been successfully fabricated by a blending and spin-coating method.

To investigate the effect of ZnO@CF on the crystal structure of the PVDF matrix, FTIR was conducted on pure PVDF and ZnO@CF/PVDF composite films. The FTIR spectra ranged from 400 cm^{-1} to 1000 cm^{-1} (Fig. 1f) showing absorption bands of pure PVDF and ZnO@CF/PVDF nanocomposite films with 2.0, 4.0, 6.0 and 8.0 wt% content of ZnO@CF, respectively. It can be seen that pure PVDF and the ZnO@CF/PVDF nanocomposite films have similar curves. The appearance of absorption bands at 479 cm^{-1} (CF_2 deformation), 510 cm^{-1} (CF_2 stretching) and 840 cm^{-1} (CH_2 rocking, skeletal C–C and CF_2 stretching) are assigned to the β-phase of PVDF, and the absorption bands at 609 cm^{-1} and 765 cm^{-1} (CF_2 skeletal bending) are evidence of a certain amount of α-phase present in each sample.[38,39] The added content of ZnO@CF composite has a significant influence on the electroactive β crystal content $F(\beta)$ for PVDF, which can be calculated with the Beer–Lambert theory formula (1):

$$F(\beta) = \frac{A_\beta}{\left(\frac{K_\beta}{K_\alpha}\right)A_\alpha + A_\beta} \times 100\% \quad (1)$$

where A_α and A_β correspond to absorption bands at 765 and 840 cm^{-1} for the α-phase and β-phase. The absorption coefficients for α- and β-phases are 6.1×10^4 and 7.7×10^4 cm^2 mol^{-1}, respectively.[40–43] The value of $F(\beta)$ for pure PVDF and ZnO@CF/PVDF composite films have been calculated with eqn (1), and the corresponding results are shown in Table 1. From Fig. 1f and Table 1, when the added content of ZnO@CF increases from 0 to 2.0 to 4.0 wt%, the values of $F(\beta)$ increase from 66.9 to 71.9 to 75.1%. This indicates that the addition of an appropriate amount of ZnO@CF is beneficial to the formation of β-phases, which may be because the accumulation of charges in the interfaces between ZnO NWs and PVDF polymer chains induces electronegative F atoms to deflect to one side and the β-phase of PVDF forms. A possible mechanism is proposed in Fig. S6.† But, as the amount of ZnO@CF continues to increase from 6.0 to 8.0 wt%, the value of $F(\beta)$ decreases from 74.7 to 68.9%. Electric charge accumulation is caused by the agglomeration of excessive ZnO@CF, which is not beneficial for deflecting the $-CF_2$ group, and the $F(\beta)$ decreases. The FTIR patterns demonstrate that the addition of an appropriate amount of "nail-raked" material like ZnO@CF could increase the content of the β-phase of PVDF. In order to further verify that the introduction of ZnO@CF has a significant effect on the conformational transition of the piezoelectric β-phase, the crystal and amorphous peaks were fitted from the corresponding XRD curves (Fig. S7†). Although the amount of β-phase calculated from the XRD pattern is slightly lower than that calculated from FTIR in our manuscript owing to the existence of errors in the fitting process, these fitting results show the same tendency in variation as the calculated result for $F(\beta)$ in our manuscript in Table S1,† which indicates that the argument that the content of β-phase varies due to the introduction of ZnO@CF is convincing.

Fig. 2a illustrates the macrostructure of the ZnO@CF/PVDF composite film PNG and the microstructure of the ZnO@CF/

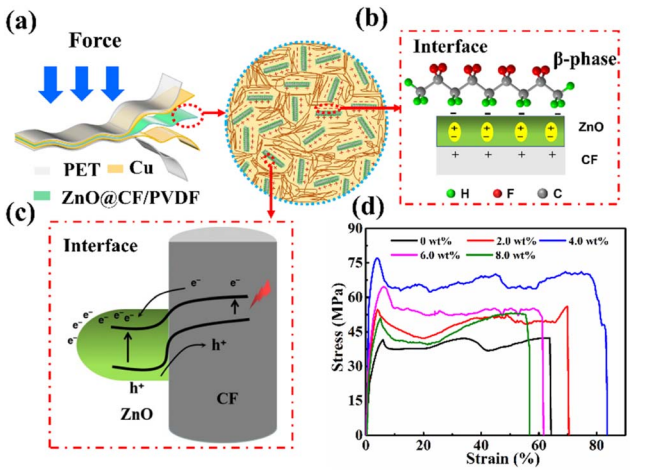

Fig. 2 (a) The macro- and micro-structures of a flexible ZnO@CF/PVDF composite film PNG. Plausible interaction mechanism of the dual interface: (b) between ZnO and PVDF; (c) between ZnO and CF. (d) The strain–stress curve of the ZnO@CF/PVDF composite film with different contents of ZnO@CF of 0, 2.0, 4.0, 6.0 and 8.0 wt%.

Table 1 Summary of parameters for pure PVDF (0 wt%) and ZnO@CF/PVDF composite films with 2.0, 4.0, 6.0 and 8.0 wt% content of ZnO@CF

ZnO@CF (wt%)	Voltage (V)	Current (μA)	ε_r (10^2 Hz)	P_r (μC cm^{-2})	d_{33} (pC N^{-1})	$F(\beta)$ (%)
0	2.71	0.15	9.59	0.48	8.32	66.91
2.0	8.27	0.58	13.93	0.66	16.28	71.90
4.0	14.90	1.25	18.82	0.98	32.65	75.06
6.0	9.09	0.81	22.09	0.82	32.07	74.70
8.0	5.72	0.60	24.53	0.62	26.93	68.87

PVDF composite film. A ZnO@CF/PVDF composite film with good flexibility could generate electric charge when an external pressure is applied to the PNG. The dual interface emerged by adding "nail-raked" ZnO@CF into the PVDF matrix: (i) the interface between ZnO and PVDF (Fig. 2b) will promote the formation of the piezoelectric β-phase. On the one hand, the ZnO NWs increase the formation of an extended chain conformation due to the existence of an electric field in the region of inter-chain spacing. On the other hand, ZnO@CF will interact with the PVDF dipoles and exists in a dormant state in the PVDF matrix.[44] Therefore, the increase in piezoelectric β-phase after mixing with ZnO@CF would result in excellent electric performance. The output performance of the ZnO@CF/PVDF composite film PNG will be discussed below. (ii) The interface between ZnO and CF (Fig. 2c) will accelerate the migration electric charge and improve the mechanical properties. First, the electron affinity of ZnO and Schottky contacts between the ends of ZnO NWs and carbon fiber is beneficial to electric charge migrating to the side of the carbon fiber.[45] The conductivity of ZnO is lower than that of CF, so Schottky contacts form a dipole layer, which would promote the migration of polarization charges close to the interface area of ZnO rods and short chopped CF. Second, an appropriate amount of "nail-raked" ZnO@CF will improve the mechanical properties and the strain–stress curves (Fig. 2d).

Fig. 2d presents the typical strain–stress curves of the ZnO@CF/PVDF composite film with different contents of ZnO@CF of 0, 2.0, 4.0, 6.0 and 8.0 wt%. The tensile strength, Young's modulus and elongation at break all increase as the content of ZnO@CF increases from 0 to 4.0 wt%, while those values decrease when the content of ZnO@CF continues to increase from 6.0 to 8.0 wt%. Detailed data for the variation in those parameters is given in Fig. S8.† The maximum values of tensile strength, Young's modulus and elongation at break of the ZnO@CF/PVDF composite film reached 77.37 MPa, 4.47 GPa and 77%, which were improvements of 85.9%, 194% and 22.3%, respectively, compared with pure PVDF film. This clearly illustrated that the dual interface between ZnO and CF and between ZnO and PVDF can effectively enhance the mechanical properties and electrical performance. The electrical performance will be discussed in detail below.

3.2 Electrical performance

To consider the flexibility and output performance of the ZnO@CF/PVDF composite film, the influence of the thickness of the composite film on output performance was investigated (Fig. S9†). The maximum output voltage value of the ZnO@CF/PVDF composite film increases linearly with thickness under the same periodic pressing test. When the thickness of the ZnO@CF/PVDF composite film is 100 μm, the output voltage achieves 14.75 V. The flexibility of ZnO@CF/PVDF composite film was also considered, so the thickness of the ZnO@CF/PVDF composite film was chosen as 100 μm and the same thickness was prepared to investigate the influence of different contents of ZnO@CF on output performance in this work.

The open-circuit voltage and short-circuit current performance of pure PVDF and ZnO@CF/PVDF composite films with different contents of ZnO@CF (2.0, 4.0, 6.0 and 8.0 wt%) are shown in Fig. 3a–c. It should be noted that the concentration of ZnO@CF in the composite film had a great influence on the piezoelectric outputs of the PENG device. Initially, the output voltages and currents of ZnO@CF/PVDF composite films gradually increased with increasing concentration of ZnO@CF. As the content of ZnO@CF increased, the voltage and current of the ZnO@CF/PVDF composite film increased and then decreased. When the ZnO@CF content increases from 0 to 2.0 and to 4.0 wt%, the output voltage of ZnO@CF/PVDF composite film increases from 2.71 to 8.47 to 14.91 V, and the output current increases from 0.15 to 0.58 to 1.25 μA, respectively. It is obvious that there is a similar variation tendency in open-circuit voltage and short-circuit current output performance with the increase in the content of ZnO@CF. Specifically, when the content of ZnO@CF went up to 4.0 wt%, the maximum output voltage and current were obtained, which were about 5.5 and 8.3 times higher, respectively, than those of pure PVDF. Additionally, when the ZnO@CF content increased from 4.0 to 6.0 to 8.0 wt%, the output voltage of the ZnO@CF/PVDF composite film decreased from 14.91 to 9.09 to 5.72 V, and the output current also decreased from 1.25 to 0.81 to 0.60 μA, respectively. The dependence of the output voltages and currents of the ZnO@CF/PVDF composite film on the ZnO@CF concentration are summarized in Table 1. The output voltage and current of the ZnO@CF/PVDF composite film PNG are higher than those of ZnO/PVDF or CF/PVDF composite film PNGs (Fig. S10 and S11†). Compared to other structural design composite film PNGs based on ZnO/PVDF doped nanocarbon materials, the output performance of the hierarchical array ZnO@CF/PVDF composite film PNG in our work is superior to that of other PNGs incorporating structural ternary (ZnO, nanocarbon materials and PVDF) in Table 2.

The variation tendencies of output performance for the ZnO@CF/PVDF composite film could be explained by percolation theory.[46–48] A certain amount of carbon material (such as acetylene black or rGO) employed as a conductive phase in a piezoelectric composite could improve the migration rate of the polarization charges, which was proved in our previous work.[46] In this work, the amount of ZnO@CF was a trade-off between the piezoelectric property and the conductive property. When the ZnO@CF content is below the threshold (ZnO@CF ~4.0 wt%), the conductive and piezoelectric properties are in synergy and the output performance increases as the addition of ZnO@CF increases. Nevertheless, when the ZnO@CF content is over a certain threshold (ZnO@CF ~4.0 wt%), the composite film tends to be conductive and the leakage current is increased.

Finally, the output performance decreases with the continued addition of ZnO@CF. Moreover, the threshold of pure CF is about 2.0 wt% in a CF/PVDF composite film (Fig. S10†), which is lower than the threshold of ZnO@CF for a ZnO@CF/PVDF composite film.

In addition, Fig. 3d shows the frequency-dependent output voltages of the ZnO@CF/PVDF composite film with an

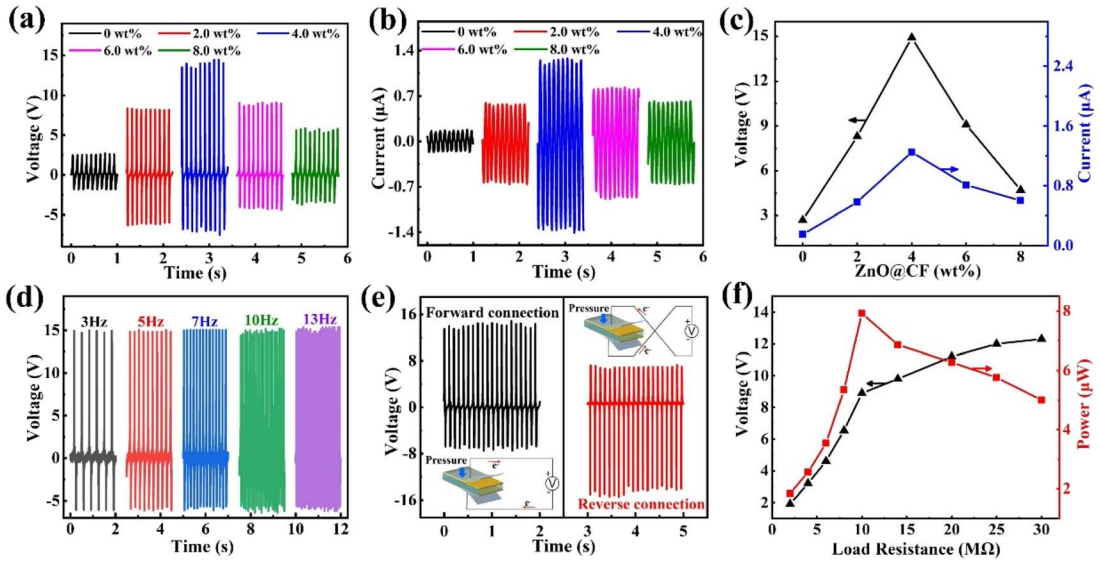

Fig. 3 Piezoelectric performance of the ZnO@CF/PVDF composite film PNG. (a) Dependence of open-circuit voltage on ZnO@CF content. (b) Dependence of short-circuit current on ZnO@CF content. (c) Diagram of the maximum values of voltage and current. (d) Open-circuit voltage of ZnO@CF/PVDF measured at different testing frequencies. (e) Open-circuit voltage of ZnO@CF/PVDF in reverse and forward connections. (f) Open-circuit voltage and instantaneous power of ZnO@CF/PVDF with different external load resistors.

operating frequency ranging from 3 to 13 Hz. With an increase in frequency from 3 to 13 Hz, the average output voltage of the ZnO@CF/PVDF composite film with 4.0 wt% ZnO@CF is maintained at 14.80 V. Under open-circuit conditions, the voltage can be expressed by the formula (2):

$$V_{oc} = k_1 \times \frac{d_{33}}{{\varepsilon_{33}}^T} \times h \times \Delta\sigma \quad (2)$$

where k_1 is a constant, d_{33} is the piezoelectric coefficient (pC N^{-1}), ${\varepsilon_{33}}^T$ is the permittivity at constant stress along the polarization direction, h is the thickness, and $\Delta\sigma$ is mechanical stress.[49] This indicates that the output performance of the PNG is unrelated to the frequency of the external compressive force and it can harvest energy from various frequencies. The output voltage of the ZnO@CF/PVDF composite film PNG increases from 7.4 to 16.1 V as the loading force varies from 5 to 20 N at a fixed frequency of 2 Hz (Fig. S12†), which indicates that the composite PNG is sensitive to the external force and can be used as a sensor. The sensitivity of the ZnO@CF/PVDF composite film sensor is calculated from the linear slope of a fitted plot of voltage *versus* force, and the slope is 0.57 V N^{-1}.

To confirm that the output signals were indeed created by the piezoelectric phenomenon of the ZnO@CF/PVDF composite film rather than from triboelectricity or an external disturbance, a switching-polarity test was carried out (Fig. 3e). A positive signal was measured when the ZnO@CF/PVDF composite film nanogenerator was forward connected in the measurement circuit. In contrast, a positive signal for the ZnO@CF/PVDF composite film nanogenerator was generated with the reverse connection under the same conditions. Moreover, the signal magnitude at pressing was higher than that under release, ascribed to the different strain rates during pressing and release. This clearly confirms that the detected outputs are the piezoelectric signals from the ZnO@CF/PVDF composite film nanogenerator during pressing and release. Furthermore, to characterize the capability of using the proposed ZnO@CF/PVDF composite film nanogenerator in practical applications, the output voltage of the ZnO@CF/PVDF composite film nanogenerator under external load resistances ranging from 1 to 30 MΩ increases from 1.92 to 12.3 V (Fig. 3f). Meanwhile, the instantaneous output power was calculated with formula (3):

Table 2 Output comparison of different structural designs for ZnO@carbon materials/PVDF PNG

Structure	Active materials	Voltage (V)	Current (μA)	Power (μW)	Ref.
Blended	ZnO-MWCNT/PVDF	8.1	4.0		50
	ZnO/GO/PVDF	14.0	0.22	3.1	51
	ZnO NPs/MWCNTs/PDMS	7.5	2.5	18.75	52
3D skeleton	ZnO@rGO/PDMS	0.5	2.0		53
Carbon-coat	Carbon dot@ZnO/PVDF-HFP	0.8			33
Multilayer	ZnO NWs/CNTs/PDMS	4.9			54
	ZnO/graphene/PET	0.17	0.0275		55
Hierarchical array	ZnO@CF/PVDF	14.9	1.25	7.92	This work

$$P = V^2/R \quad (3)$$

where V is the output voltage of the ZnO@CF/PVDF composite film and R is the corresponding external load resistance. The maximum output power is calculated to be about 7.9 μW with an external load of 10 MΩ. It is known that, when the internal resistance of the nanogenerator is equal to the external load resistance, the output power will achieve its maximum value. Therefore, the internal resistance of the ZnO@CF/PVDF composite film nanogenerator is about 10 MΩ.

To effectively reveal the effect of the ZnO@CF on the piezoelectric output performance of the ZnO@CF/PVDF composite film nanogenerator, the dielectric properties (ε_r) in a frequency range from 10^2 to 10^6 Hz and the remanent polarization (P_r, μC cm^{-2}) of the samples at typical room temperature (~25 °C) were investigated (Fig. 4). From Fig. 4a: (i) note that the ε_r of the pure PVDF film and ZnO@CF/PVDF composite film with different contents of ZnO@CF (2.0, 4.0, 6.0 8.0 wt%) gradually decreases as the frequency increases. This is attributed to the high interfacial polarization at the conductor–insulator interface originating from the Maxwell–Wagner–Sillars polarization effect,[56] which would cause the accumulation of charge carriers at the interface and relaxation polarization. (ii) The ε_r of all ZnO@CF/PVDF composite film samples are higher than that of pure PVDF, and those values of ε_r gradually increase as the ZnO@CF content increases from 2.0 to 4.0 to 6.0 to 8.0 wt%. For ZnO@CF/PVDF composite films, as the content of ZnO@CF increases from 2.0 to 8.0 wt%, the value of ε_r increases from 13.9 to 24.5 at a frequency of 100 Hz, and those values are higher than that of pure PVDF, which may be ascribed to the greater interfacial and ionic polarization introduced by ZnO@CF.[57] The dielectric constant from the fitted curve at different frequencies (10^2 to 10^6 Hz) and the data for the doping content of ZnO@CF (Fig. 4b) are summarized in Table S2.† The ε_r increases linearly as the content of ZnO@CF varies from 0 to 8.0 wt% (Fig. 4b). The dielectric loss ($\tan\delta$) values of all the ZnO@CF/PVDF composite films were low and under 0.5, and those of the ZnO@CF/PVDF composite film are lower than that of pure PVDF (Fig. S13†). This indicates that the synthesized composite nanofiber films with high ε_r and low $\tan\delta$ are imbued with excellent charge storage capability.

The polarization–electric field (P–E) loops of pure PVDF and ZnO@CF/PVDF composite films were measured at room temperature 25 °C (Fig. 4c and d). From Fig. 4c and d: (i) the remanent polarization P_r increases from 0.48 to 0.66 to 0.98 μC cm^{-2} as the content of ZnO@CF increases from 0 to 2.0 to 4.0 wt%. When the content of ZnO@CF increases from 6.0 to 8.0 wt%, the P_r value decreases from 0.82 to 0.62 μC cm^{-2} (Fig. S14†). (ii) The maximum polarization increases from 0.39 to 0.60 to 0.75 μC cm^{-2} as the content of ZnO@CF increases from 0 to 2.0 to 4.0 wt%. While the content of ZnO@CF increases from 6.0 to 8.0 wt%, the maximum polarization decreases from 0.62 to 0.56 μC cm^{-2} (Fig. S15†). Those results demonstrate that

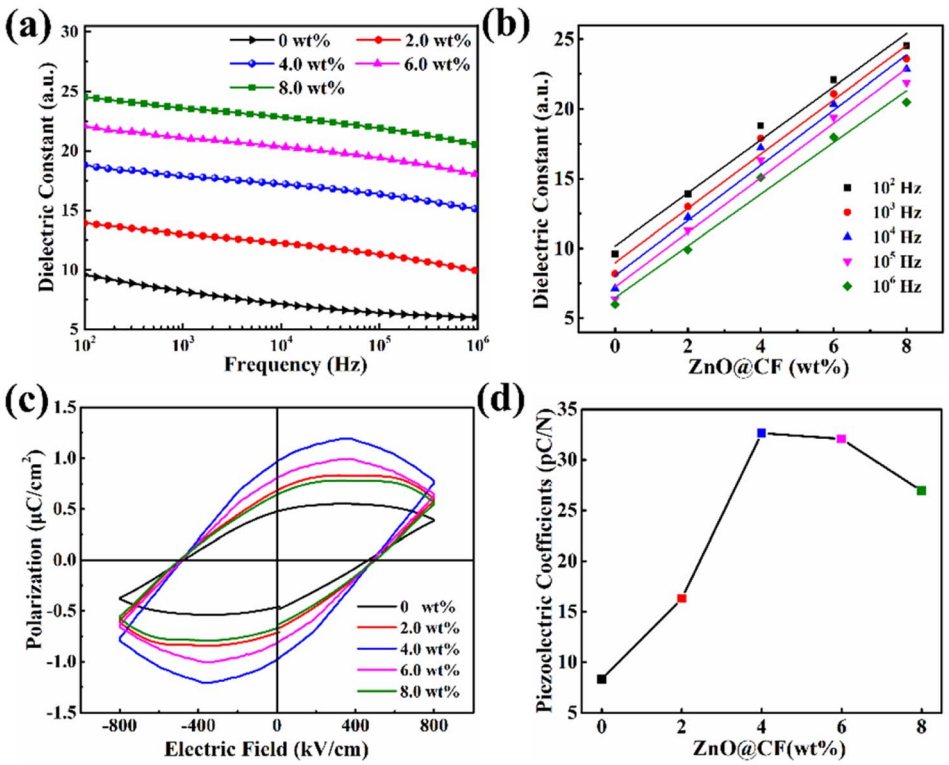

Fig. 4 Piezoelectric parameters for ZnO@CF/PVDF composite film. (a) Dependence of dielectric constant on frequency at room temperature (25 °C). (b) Fitted curves for a plot of dielectric constant at different frequencies and doping contents of ZnO@CF. (c) Polarization–electric field hysteresis loops (P–E) at room temperature (25 °C). (d) Diagram of the residual polarization (P_r) varying with doping content of ZnO@CF.

ZnO@CF could enhance the remanent polarization and maximum intensity of the composite piezoelectric film.

It is known that the output performance of piezoelectric materials is determined by the piezoelectric coefficient d_{33}, and d_{33} can be calculated with formula (4):

$$d_{33} = 2Q_{11}\varepsilon_0\varepsilon_r P_r \quad (4)$$

where ε_0 is the permittivity of a vacuum ($\varepsilon_0 = 8.854 \times 10^{-12}$ F m^{-1}), and Q_{11} is the electrostrictive constant of the paraelectric phase (0.05–0.1 m^4 C^{-2}. To simplify calculation, Q_{11} was chosen as 0.1 m^4 C^{-2}),[13,26] and the value of ε_r was chosen as the value measured at a frequency of 100 Hz. According to eqn (3), the d_{33} value *versus* ZnO@CF content is shown in Fig. 4d. The value of d_{33} increases from 8.32 to 16.28 to 32.65 pC N^{-1} when the content ZnO@CF increases from 0 to 2.0 to 4.0 wt%. However, as the content of ZnO@CF further increases from 6.0 to 8.0 wt%, d_{33} decreases from 32.07 to 26.93 pC N^{-1}. This result is a good justification of the variation rule for output voltage and current for a ZnO@CF/PVDF composite film PNG (Fig. 3a–c and Table 1).

3.3 Stability and application

To further evaluate the feasibility of energy harvesting for the purpose of powering electronic devices, the ZnO@CF/PDVF composite film PNG was employed to charge a capacitor (10 μF) through a bridge rectified circuit, and the capacitor as a power source can drive a commercial LED when the capacitor is discharged (Fig. 5a). When the control switch S is closed to A, the rectified output power charges the energy storage capacitor; but, if the switch is turned to B, the capacitor is discharged and the commercial red LED is illuminated. The charging voltage for the 10 μF capacitor reached 4.0 V in about 500 s, and the capacitor discharged to 3.15 V to light the LED instantaneously within 1 second. The capacitor can continuously charge from 3.15 V to 4.0 V, and charge and discharge can be repeated to turn on and off an LED light. An enlarged view of the discharging process is shown in Fig. S16.† The bridge rectifier can convert the AC signal into a DC signal, and then the output electrical signal is collected by an oscilloscope. The output signal after rectification is shown in Fig. 5b, and the inset images show the signal before and after rectification. Moreover,

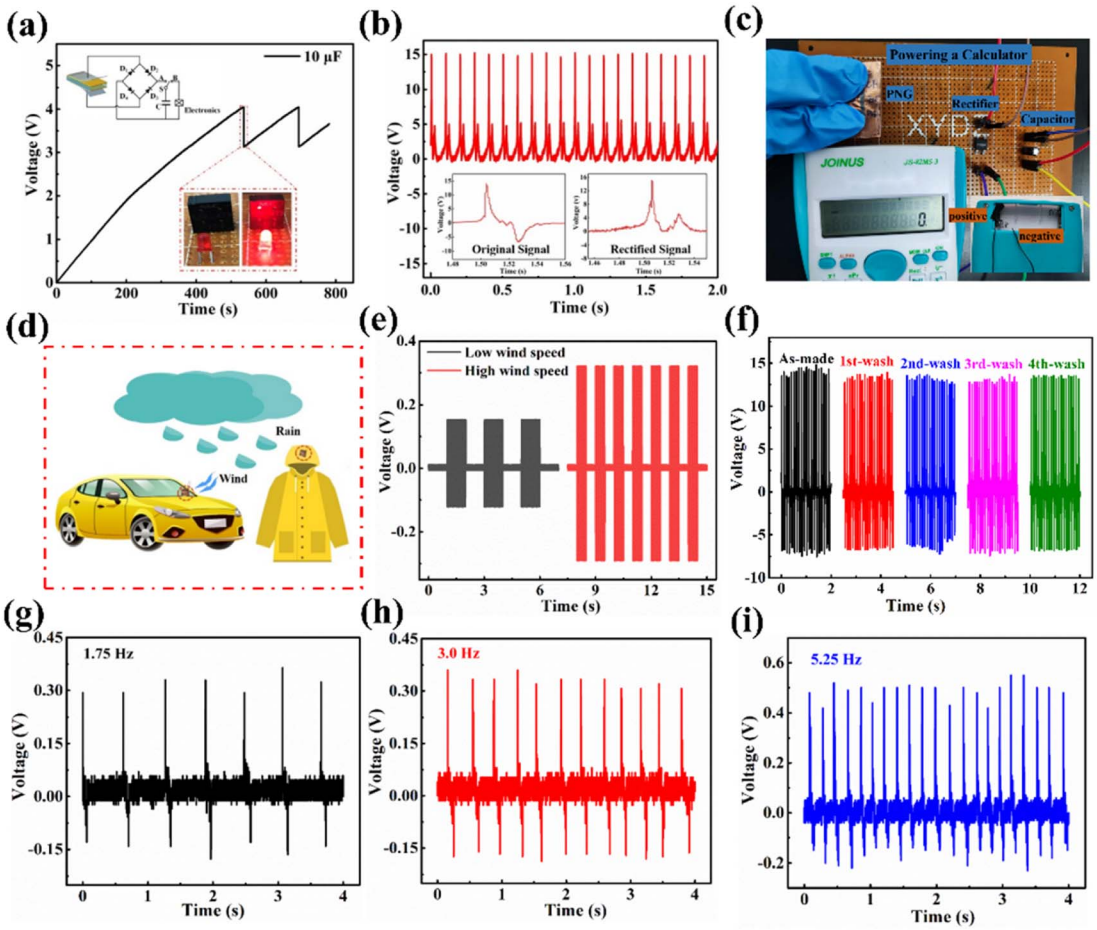

Fig. 5 Application of a typical PNG based on a ZnO@CF/PVDF with 4.0 wt% of ZnO@CF. (a) Charging and discharging voltage of capacitor: upper-left inset image: a schematic circuit diagram; lower-right insert image: a red LED illuminated by the PNG. (b) Rectified output voltage of the PNG. (c) Photograph of a commercial calculator driven by the ZnO@CF/PVDF composite PNG. (d) Schematic of the ZnO@CF/PVDF composite PNG applied to outdoor clothing and vehicles in windy and rainy weather. (e) Electrical response of the piezoelectric sensor to wind speed. (f) Water-washable experience for PNG for one to four times; water drops falling at different frequencies: (g) 1.75 Hz; (h) 3.0 Hz; (i) 5.25 Hz.

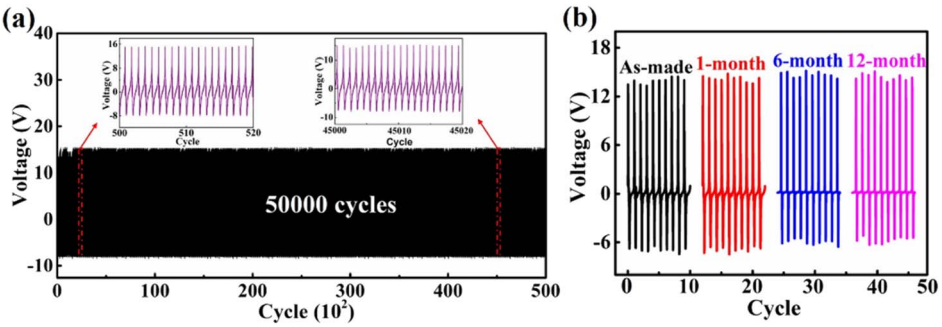

Fig. 6 (a) Durability dependence on periodic pressing-release test of the ZnO@CF/PVDF composite PNG for 50 000 cycles. (b) Test of dependence of stability on time for the ZnO@CF/PVDF composite PNG over 12 months.

the energy harvested from the ZnO@CF/PDVF composite PNG after bridge rectification could drive a commercial calculator and the circuit is shown in Fig. 5c. These results well indicate that our prepared ZnO@CF/PDVF composite film PNG can be considered an efficient and promising power source for low energy consumption electronic devices by converting mechanical energy into electricity.

A ZnO@CF/PVDF composite film PNG could be pasted on the surface of vehicles or raincoats to monitor weather, such as wind or rainfall in an outdoor environment (Fig. 5d). In order to test wind velocity, the response of the ZnO@CF/PDVF composite film PNG sensor to different wind speeds was studied and the results are shown in Fig. 5e. Periodical wind was simulated and generated by a hair dryer and the output signal of the ZnO@CF/PDVF composite film PNG sensor under periodical simulated wind was acquired with a test system whose building and circuit diagram are shown in Fig. S17.† The output voltage of the designed flexible ZnO@CF/PDVF composite sensor can clearly distinguish different wind speeds from an electric hair dryer (Fig. 5e). The output voltage increased with wind speed: the output voltage of the ZnO@CF/PDVF composite sensor is 0.16 V at low wind speed, and that value is 0.31 V at high wind speed. This is due to the increasing wind speed generating a higher impact force on the piezoelectric film surface. The waterproof properties of composite films should also be considered before use as a rainfall sensor. Fig. 5f shows the output voltage of a ZnO@CF/PDVF composite sensor washed in deionized water for 15 min at a time. From Fig. 5f, the output voltage of the ZnO@CF/PDVF composite sensor shows a slight decline in comparison with that of the as-made sensor, which demonstrates it processes good waterproof properties, and it has the potential to be used as a rainfall sensor.

In order to monitor rainfall intensity, the response of the ZnO@CF/PDVF composite piezoelectric sensor to different frequencies of water drops was measured (Fig. 5g–i). Rainfall was simulated by changing the falling rate of the water droplets, and the output signal of the ZnO@CF/PDVF composite film PNG sensor under rainfall and wind was acquired *via* a test system built in our lab, the circuit diagram for which is shown in Fig. S17.† The average output voltage of the ZnO@CF/PDVF composite sensor increases as the falling rate of the water drops increases, and those values are 0.32 V, 0.41 V and 0.52 V under 1.75 Hz, 3.0 Hz and 5.25 Hz, respectively. This is due to the higher frequency of water drops causing a higher impact force from falling raindrops; therefore, the ZnO@CF/PDVF composite sensor can distinguish different intensities of rainfall and it has the potential to be used as a rain weather sensor to monitor outdoor raindrops.

To verify the mechanical durability and stability of the as-prepared ZnO@CF/PVDF composite PNG, a periodic pressing-release test was carried out for a large number of cycles and for a long time (Fig. 6). The mechanical durability of the as-prepared ZnO@CF/PVDF composite PNG was demonstrated by the periodic pressing-release test for 50 000 cycles. As illustrated in Fig. 6a, it can be observed that there is no fluctuation or attenuation in the output voltages of the ZnO@CF/PVDF composite PNG even after 50 000 cycles of repeated loading tests, revealing the excellent mechanical durability of the ZnO@CF/PVDF composite PNG. To test the tolerance for long-term exposure to an ambient environment of the ZnO@CF/PVDF composite PNG, a test of the dependence of stability on time was undertaken for 12 months and the results are shown in Fig. 6b. From Fig. 6b, compared to the as-made PNG device, the output peak–peak voltage of the ZnO@CF/PVDF composite PNG shows small drops of 0.28%, 2.40% and 3.94% after one month, six months and twelve months, respectively, revealing the stability of the ZnO@CF/PVDF composite structure. These results indicate that the ZnO@CF/PVDF composite PNG has capacity for application as a sensor or for harvesting mechanical energy due to its durability and stability.

4. Conclusions

In summary, this work demonstrates a novel strategy to construct a flexible, lead-free, low-cost and washable PNG based on a hierarchical ZnO@CF/PVDF composite film for a piezoelectric meteorological sensor. Hexagonal ZnO NWs have been successfully grown over the entire CF surface and the average diameter of ZnO NWs is 150 nm. The fraction of the β-phase of the ZnO@CF/PVDF composite film reached 75.06% as the content ZnO@CF increased from 4.0 wt% to 12.2% compared to a pure PVDF film. The output voltage and current of the ZnO@CF/PVDF composite film PNG with a ZnO@CF content of 4.0 wt% achieved 14.9 V and 1.25 μA, which were improvements

of 7.3 and 4.5 times compared with those of a pure PVDF PNG. The peak power of the ZnO@CF/PVDF PNG is 7.92 μW with an external load of 10 MΩ. The calculated d_{33} of the ZnO@CF/PVDF composite film also reached a maximum value of 32.65 pC N^{-1} when the content of ZnO@CF was 4.0 wt%. The composite PNG could charge a capacitor and light up an LED and drive a commercial calculator when the capacitor discharged. More interestingly, this ZnO@CF/PVDF composite film PNG demonstrated its competency for monitoring meteorological weather such as wind and rainfall, and the output voltage of the ZnO@CF/PVDF composite PNG maintained excellent durability and stability after 50 000 cycles of mechanical beating and 12 months of tolerance to an ambient environment. This work demonstrates an effective approach to fabricating a flexible PNG with excellent performance, and provides further enlightenment for the rapid progress of meteorological sensors, smart clothes and vehicles.

Author contributions

Yinhui Li: conceptualization, methodology, visualization, writing-original draft, funding acquisition. Jiaojiao Sun: data curation, formal analysis, writing-review & editing. Pengwei Li: conceptualization, validation, funding acquisition. Xuran Li: validation, writing-review & editing. Jianqiang Tan: validation, formal analysis. Hulin Zhang: supervision, validation. Tingyu Li: supervision, funding acquisition. Jianguo Liang: supervision, validation, funding acquisition. Yunlei Zhou: supervision, funding acquisition. Zhenyin Hai: supervision, writing – review & editing. Jin Zhang: supervision, funding acquisition, writing – review & editing.

Conflicts of interest

The authors declare no conflicts of interest.

Acknowledgements

This work was supported by National Natural Science Foundation of China (Grant No. 52075361, No. 52205593), Major Science and Technology Project of Shanxi Province (20201102003), Key Research and Development Projects in Shanxi Province (201903D421030), the Shanxi Province Science Foundation for Youths (Grant No. 20210302124046), the National Science Foundation of Shanxi Province (Grant No. 20210302123156, 20210302123157), the Scientific and Technological Innovation Programs of Higher Education Institutions in Shanxi (Grant No. 2019L0243).

References

1 Z. Zhao, J. Wang, C. Fu, Z. Liu, D. Liu and B. Li, *J. Sens.*, 2018, **2018**, 1–13.
2 A. Sharma, Y. Kumar, K. Mazumder, A. K. Rana and P. M. Shirage, *New J. Chem.*, 2018, **42**, 8445–8457.
3 G. Chen, Q. Feng and J. Wang, *Sci. Total Environ.*, 2020, **703**, 135504.
4 Q. Zhang, W. Smith and M. Shao, *Remote Sens.*, 2023, **15**, 886–890.
5 R. Babari, N. Hautière, É. Dumont, N. Paparoditis and J. Misener, *Transp. Res. Part C Emerg. Technol.*, 2012, **22**, 17–28.
6 Z. L. Wang and J. Song, *Science*, 2006, **312**, 242–246.
7 X. Guan, B. Xu and J. Gong, *Nano Energy*, 2020, **70**, 104516.
8 M. A. Johar, A. Waseem, M. A. Hassan, I. V. Bagal, A. Abdullah, J. S. Ha and S. W. Ryu, *Adv. Energy Mater.*, 2020, **10**, 2002608–2002618.
9 M. Zhu, Q. Shi, T. He, Z. Yi, Y. Ma, B. Yang, T. Chen and C. Lee, *ACS Nano*, 2019, **13**, 1940–1952.
10 B. Moorthy, C. Baek, J. E. Wang, C. K. Jeong, S. Moon, K.-I. Park and D. K. Kim, *RSC Adv.*, 2017, **7**, 260–265.
11 K. Maity, S. Garain, K. Henkel, D. Schmeißer and D. Mandal, *ACS Appl. Polym. Mater.*, 2020, **2**, 862–878.
12 C. K. Jeong, D. Y. Hyeon, G. T. Hwang, G. J. Lee, M. K. Lee, J.-J. Park and K. I. Park, *J. Mater. Chem. A*, 2019, **7**, 25481–25489.
13 X. Li, Y. Li, Y. Li, J. Tan, J. Zhang, H. Zhang, J. Liang, T. Li, Y. Liu, H. Jiang and P. Li, *ACS Appl. Mater. Interfaces*, 2022, **14**, 46789–46800.
14 M. Zhang, T. Gao, J. Wang, J. Liao, Y. Qiu, H. Xue, Z. Shi, Z. Xiong and L. Chen, *Nano Energy*, 2015, **11**, 510.
15 G. Jian, Y. Jiao, Q. Meng, Y. Guo, F. Wang, J. Zhang, C. Wang, K. S. Moon and C. P. Wong, *Nano Energy*, 2021, **82**, 778.
16 V. Singh, D. Meena, H. Sharma, A. Trivedi and B. Singh, *Energy*, 2022, **239**, 122125–122135.
17 L. Yang, Q. Zhao, K. Chen, Y. Ma, Y. Wu, H. Ji and J. Qiu, *ACS Appl. Mater. Interfaces*, 2020, **12**, 11045–11054.
18 S. Bairagi and S. W. Ali, *Soft Matter*, 2020, **16**, 4876–4886.
19 J. Li, C. M. Zhao, K. Xia, X. Liu, D. Li and J. Han, *Appl. Surf. Sci.*, 2019, **463**, 626–634.
20 M. Sahu, S. Hajra, K. Lee, P. L. Deepti, K. Mistewicz and H. J. Kim, *Crystals*, 2021, **11**, 85–95.
21 S. Azimi, A. Abolhasani, S. M. Moosavi, F. Vanaei, A. Jafari, E. Samimi-Sohrforozani, M. T. Rayati, E. Noori, E. Rafiee, A. Javadi and M. M. Abolhasani, *ACS Appl. Electron. Mater.*, 2021, **3**, 4689–4698.
22 S. Ippili, V. Jella, J.-H. Eom, J. Kim, S. Hong, J. S. Choi, T. Van-Dang, H. Nguyen Van, Y.-J. Kim, H.-J. Kim and S.-G. Yoon, *Nano Energy*, 2019, **57**, 911–923.
23 R. Bhunia, S. Das, S. Dalui, S. Hussain, R. Paul, R. Bhar and A. K. Pal, *Appl. Phys. A*, 2016, **122**, 637–650.
24 B. Sun, X. Li, R. Zhao, H. Ji, J. Qiu, N. Zhang, D. He and C. Wang, *J. Mater. Sci.*, 2018, **54**, 2754–2762.
25 H. Parangusan, D. Ponnamma and M. A. A. Al-Maadeed, *Sci. Rep.*, 2018, **8**, 754–765.
26 M. Xia, C. Luo, X. Su, Y. Li, P. Li, J. Hu, G. Li, H. Jiang and W. Zhang, *J. Mater. Sci.: Mater. Electron.*, 2019, **30**, 7558–7566.
27 S. Q. Zhang, Y. S. Gao, G. Z. Zhao, Y. J. Yu, M. Chen and X. F. Wang, *Compos. Struct.*, 2020, **234**, 111694–111704.
28 M. Hasanzadeh, M. R. Ghahhari and S. M. Bidoki, *J. Mater. Sci.: Mater. Electron.*, 2021, **32**, 15789–15800.
29 H. W. Mi, Y. T. Wang, H. Chen, L. N. Sun, X. Z. Ren, Y. L. Li and P. X. Zhang, *Nano Energy*, 2019, **66**, 104136.

30 R. Bhunia, S. Gupta, B. Fatma, Prateek, R. K. Gupta and A. Garg, *ACS Appl. Mater. Interfaces*, 2019, **11**, 38177–38189.
31 Y. S. Tan, K. Yang, B. Wang, H. Li, L. Wang and C. X. Wang, *Nano Res.*, 2021, **14**, 3969–3976.
32 E. S. Nour, A. Khan, O. Nur and M. Willander, *Nanomater. Nanotechnol.*, 2014, **4**, 24.
33 P. Huang, S. Xu, W. Liu, C. Liu, H. Ou, Y. Luo, Z. Yan, X. Zhou, P. Wu and X. Liao, *ACS Appl. Mater. Interfaces*, 2023, **15**, 6735–6746.
34 X. Li, D. Ji, B. Yu, R. Ghosh, J. He, X. Qin and S. Ramakrishna, *Chem. Eng. J.*, 2021, **426**, 130345.
35 C. Luo, S. Hu, M. Xia, P. Li, J. Hu, G. Li, H. Jiang and W. Zhang, *Energy Technol.*, 2018, **6**, 922–927.
36 A. Hassanpour, N. Bogdan, J. A. Capobianco and P. Bianucci, *Mater. Des.*, 2017, **119**, 464–469.
37 K. Nakamura, S. Higuchi and T. Ohnuma, *J. Appl. Phys.*, 2016, **119**, 114102–114113.
38 P. Thakur, A. Kool, N. A. Hoque, B. Bagchi, F. Khatun, P. Biswas, D. Brahma, S. Roy, S. Banerjee and S. Das, *Nano Energy*, 2018, **44**, 456–467.
39 L. L. Ye, L. Y. Chen, J. L. Yu, S. J. Tu, B. Yan, Y. H. Zhao, X. Bai, Y. C. Gu and S. Chen, *J. Mater. Sci.: Mater. Electron.*, 2021, **32**, 3966–3978.
40 T. Lei, L. Yu, G. Zheng, L. Wang, D. Wu and D. Sun, *J. Mater. Sci.*, 2015, **50**, 4342–4347.
41 H. H. Singh and N. Khare, *Nano Energy*, 2018, **51**, 216–222.
42 S. Zeng, M. Zhang, L. Jiang, Z. Wang, H. Gu, J. Xiong, Y. Du and L. Ren, *ACS Appl. Mater. Interfaces*, 2022, **14**, 7990–8000.
43 W. J. Oh, H. S. Lim, J. S. Won and S. G. Lee, *Polymers*, 2018, **10**, 1333–1334.
44 S. Pratihar, A. Patra, A. Sasmal, S. K. Medda and S. Sen, *Soft Matter*, 2021, **17**, 8483–8495.
45 X. Xue, W. Zang, P. Deng, Q. Wang, L. Xing, Y. Zhang and Z. L. Wang, *Nano Energy*, 2015, **13**, 414–422.
46 Y. Li, J. Tan, K. Liang, Y. Li, J. Sun, H. Zhang, C. Luo, P. Li, J. Xu, H. Jiang and K. Wang, *J. Mater. Sci.: Mater. Electron.*, 2022, **33**, 4291–4304.
47 Z. M. Dang, C. W. Nan, D. Xie, Y. H. Zhang and S. C. Tjong, *Appl. Phys. Lett.*, 2004, **85**, 97–99.
48 M. Rahaman, T. K. Chaki and D. Khastgir, *Compos. Sci. Technol.*, 2012, **72**, 1575–1580.
49 Y. Zhang, M. Wu, Q. Zhu, F. Wang, H. Su, H. Li, C. Diao, H. Zheng, Y. Wu and Z. L. Wang, *Adv. Funct. Mater.*, 2019, **29**, 1904259.
50 A. R. Chowdhury, A. M. Abdullah, I. Hussain, J. Lopez, D. Cantu, S. K. Gupta, Y. Mao, S. Danti and M. J. Uddin, *Nano Energy*, 2019, **61**, 327–336.
51 E. S. Kadir and R. N. Gayen, *Sens. Actuators, A*, 2022, **333**, 113305.
52 H. Sun, H. Tian, Y. Yang, D. Xie, Y. C. Zhang, X. Liu, S. Ma, H. M. Zhao and T. L. Ren, *Nanoscale*, 2013, **5**, 6117–6123.
53 X. Li, Y. Chen, A. Kumar, A. Mahmoud, J. A. Nychka and H. J. Chung, *ACS Appl. Mater. Interfaces*, 2015, **7**, 20753–20760.
54 C. Jin, L. Dong, Z. Xu, A. Closson, A. Cabe, A. Gruslova, S. Jenney, D. Escobedo, J. Elliott, M. Zhang, N. Hao, Z. Chen, M. D. Feldman and J. X. J. Zhang, *Adv. Mater. Interfaces*, 2021, **8**, 2100094.
55 D. M. Shin, E. L. Tsege, S. H. Kang, W. Seung, S. W. Kim, H. K. Kim, S. W. Hong and Y. H. Hwang, *Nano Energy*, 2015, **12**, 268–277.
56 Y. Li, X. Su, K. Liang, C. Luo, P. Li, J. Hu, G. Li, H. Jiang and K. Wang, *Microelectron. Eng.*, 2021, **1**, 244–246.
57 X. M. Meng, X. J. Zhang, C. Lu, Y. F. Pan and G. S. Wang, *J. Mater. Chem. A*, 2014, **2**, 18725–18730.